SECED 2023 Conference
Earthquake Engineering & Dynamics for a Sustainable Future
14-15 September 2023, Cambridge, UK

SEISMIC RISK ASSESSMENT OF TYPICAL AGEING INUDSTRIAL STEEL STRCUTURES: CASE-STUDY

Armin MAJIDIAN[1] & Luigi DI SARNO[2]

Abstract: *This study investigates the evaluation of the effects that corrosion on the performance of steel industrial infrastructures with ageing effects. In this paper, a probabilistic risk assessment method is presented in relation to a case study of a real petrochemical structure located in an atmospheric environment with a high severity of corrosion. The findings of the damage assessment that were derived from the refined fragility analyses showed that long-term corrosion mass reduction has the potential to increase the probability of damage to the structure subjected to both near and far-field ground motion records. The structural seismic risk assessment showed that the corrosion can increase the annual failure rate due to the earthquake motions. The findings of this study can help owners and insurance companies make more accurate predictions regarding the damage, and as a result, they can provide an effective roadmap for the management of industrial assets.*

Introduction

Corrosion-induced damage can have a significant impact on the performance of steel structures and result in enormous costs for rehabilitation and repair of corroded elements. According to research conducted by the National Association of Corrosion Engineers (NACE) in 2016, the annual global corrosion cost was estimated to be approximately US$2.5 trillion, which represented approximately 3.4% of the global gross domestic product (GDP) in 2013 (Bowman et al., 2016). As mentioned in this study, nearly half of the global cost of corrosion damage is attributable to industry economics. For example, this cost is around 57% of the overall cost of corrosion in the European region, and in the United States, infrastructure corrosion accounts for about 17% of the overall cost of the industry sector.

Severe corrosion damage over a long period can modify the response characteristics of the building, cause a loss of mass and increase the vulnerability of the structure subjected to severe loading conditions (Wang et al., 2021, 2018; Xu et al., 2019, 2016). The seismic performance will be affected due to these structural modifications. As shown by Eq. **Error! Reference source not found.**, the corrosion rate is directly proportional to the corrosion mass loss.

$$D = \frac{W}{\rho . A} \tag{1}$$

where D is the corrosion thickness loss (in millimetre or micrometre), W is the mass loss (g), ρ and A are the density of the material and exposed area, respectively.

As corrosion loss over the lifetime of the structure is the greatest concern for engineers, time-dependent corrosion thickness loss models have been developed using experimental research data collected over exposure time. (Landolfo et al., 2010; Rizzo et al., 2019). In such models, uniform thickness loss over the entire metal surface as the most common form of corrosion in the long run was considered as shown in Eq. (2):

$$d(t) = A . t^{B} \tag{2}$$

where A is the first-year corrosion rate, B is the long-term impact coefficient, and d(t) is the thickness loss of the corroded element over time (t). Note that environmental parameters, including the presence of pollutants such as sulphur dioxide (SO_2), chloride ion (CL^-), relative humidity (RH), and temperature, affect the value of the A and B coefficients (Benarie and Lipfert, 1986; Feliu et al., 1993a, 1993b).

[1] Mr, University of Liverpool, Liverpool, United Kingdom, A.majidian@liverpool.ac.uk
[2] Dr, University of LIverpool, Liverpool, United Kingdom, Luigi.Di-Sarno@liverpool.ac.uk

The International Organization for Standardization (ISO) report in 2012, categorized corrosivity into six levels, starting from C1 for areas with minimal pollutants and low corrosion rate to CX for coastal and offshore regions with high levels of contaminants and exposure to sea salt spray with high salinity. Several researchers suggested similar models utilising Eq. (2) to estimate the A and B values by analysing the interactions between multiple environmental attacks (Kee Paik et al., 1998; Soares and Garbatov, 1999). Determining the susceptibility of structures to damage resulting from corrosion at different stages is still a matter of discussion.

In this paper, after a brief review of the mechanism of corrosion in severe environmental conditions, the damage assessment of corroded structure during the life of the structure is addressed as follows: First, the corrosion effect was modelled using Finite Element (FE) methods of a steel petrochemical plant as a case study located in a high corrosivity level zone based on the available time-dependent models in the literature. The damage states were then determined based on the proposed methodology in literature. To determine the probability of damage at various intensity measures, the median, 16 and 84 percentiles of the fragility functions were obtained. For risk evaluation, median fragility curve was utilized in conjunction with hazard characteristics specific to the location of the case study.

Corrosion mechanism

The ISO report has classified C5 category as an area with a high rate of corrosivity, particularly in coastal and industrial buildings with a high level of pollutants. Table 1 provides information on the ISO report regarding pollutant and corrosion rates at the C5 level in industrial outdoor environments. This table illustrates the range of significant environmental factors that affect corrosion rates, including the presence of industrial plant emissions such as PM10 and So_2, and airborne sea spray-derived chloride ions (PM10). The duration of time that a metal surface remains wet during atmospheric exposure is known as the time of wetness (TOW).

Description	Symbol	Annual average rate	Unit
Sulphur deposition	So_2	50~400	µg/m3
Chloride deposition	Cl^-	300~1,500	µg/m3
Particles	PM10	30~70	µg/m3
Time of wetness	TOW	2,500~5,500	hour/year
First-year corrosion rate	A	80~200	µm/year

Table 1. pollutants and corrosion rate at C5 level of corrosivity

Eq (3) represents a time-dependent model proposed by ISO (2012) to determine the corrosion thickness loss during the lifetime of the structure assuming a linear corrosion rate after 20 years of exposure.

$$d(t) = \begin{cases} At^B, & t \leq 20 \\ A\,[20^B + B(20^{B-1}) * (t-20)], & t > 20 \end{cases} \quad (3)$$

Corrosion protection techniques

The ISO report suggests that the cost of corrosion can be reduced by 15% to 35% by adopting effective corrosion management techniques and appropriate design. Structures lacking proper corrosion maintenance plans must be repaired to improve the performance of corroded elements. Traditional rehabilitation techniques, such as adding a plate to damaged portions, can increase the structure's weight and cost remarkably. Prevention strategies, such as using corrosion-resistant materials like stainless steel during the design phase, can help minimize situations that contribute to corrosion. Inhibitors can be applied as a passivation layer to prevent electrochemical reactions between the metal and the environment. Cathodic protection can convert the active (anode) parts of the metal surface to passive (cathode) and protect the metal. Coating is the most common corrosion protection method that acts as a barrier system to shield the metal from environmental attacks. CFRP (Carbon Fiber Reinforced Polymer), a lightweight and easy-to-install material, can be used to reinforce damaged components by attaching it to the damaged parts through an adhesive. Several studies have evaluated corroded elements using CFRP

products (Elchalakani, 2016; Jagtap and Pore, 2021; Yousefi et al., 2021). The experiments conducted demonstrated that the utilization of CFRP products can significantly enhance the durability and strength of the damaged element. The selection of an appropriate protective strategy depends on various factors such as the project's size, initial investment budget, accessibility, etc.

Many existing corrosion models do not consider the impact of corrosion protection methods on overall corrosion loss. However, in reality, corrosion can begin when the coating layer first gets scratched, leading to pit growth and eventual general corrosion over time as shown in Fig. 1-a. Once a corrosion product layer (rust) entirely forms on the metal surface, the corrosion rate decelerated and will be nearly zero over time. If a protective coating system is absent, the corroded components must be repaired or replaced by the end of the structure's design life. For simplicity in calculations, it is commonly assumed that the coating life, t_c, is equivalent to the initiation of uniform corrosion, t_a (Qin and Cui, 2003).

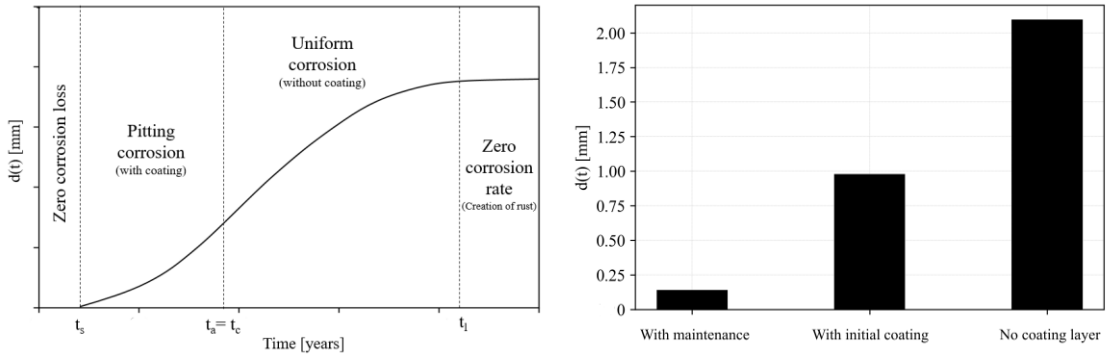

(a) (b)

Figure 1. Time-dependent corrosion model: (a) mechanism of corrosion (b) coating layer effect.

The coating system is often a practical choice for safeguarding structures against corrosion due to its ease of installation. Kere and Huang, (2019), proposed a time-dependent model to estimate the rate of corrosion over time while considering the interaction between metal corrosion and coating layer deterioration.

$$d(t) = \begin{cases} \frac{1}{A_0}\int_0^t d(t-\tau)\,.A'_l(\tau).d\tau\,, & t < tc \\ \frac{1}{A_0}\int_0^{tc} d(t-\tau)\,.A'_l(\tau).d\tau\,, & t \geq tc \end{cases} \quad (4)$$

where A_0 and $A'_l(t)$ represent the initial and rate of corrosion area loss, respectively (Kallias et al., 2016). In this model, the degradation of the coating layer is directly related to the loss of metal corrosion before the entire surface coating layer is lost (t_c). Once the coating layer is completely deteriorated, only the metal will continue to deteriorate.

Having an accurate estimation of the coating layer's service life can serve as a basis for implementing a more efficient maintenance strategy (Helsel and Lanterman, 2022). An effective maintenance plan for coating layers should be based on the practical life (P) of the protective layer, which is the point when 5 to 10% of its effectiveness is lost. Three stages can be considered for maintenance: touch-up at P for minor damage and small surface defects, maintenance repaint after 1.5*P for recoating of damaged parts, and thorough painting after 2*P for removing the existing coating and repainting.

As illustrated in Figure 1-b, a comparison of various corrosion models after 50 years of the structure's lifespan reveals a significant contrast between the mass loss of the protected (coated) and unprotected models. In fact, the difference in the absence of a coating layer is nearly 15 times greater compared to when a maintenance plan is implemented during the design life of the structure.

Methodology

Case study

A case study was conducted on a petrochemical plant structure located in the Caribbean region, close to the sea with high rate of humidity. The studied structure had a height of 61 meters, an irregular shape, and was equipped with a piping system running along its entire height, in addition to storage tanks. The study aimed to investigate the impact of corrosion on the seismic performance of the main structure of the system. The lateral resistance system consisted of ordinary braced frames in the X direction and ordinary moment frames in the Y direction. The structure was constructed using normal carbon steel material with a grade of A36, which has an expected yield and ultimate strength of 372.32 MPa and 439.89 MPa, respectively, and an elasticity module of 203 GPa. To provide context, the soil class was classified as D, and the structure had a spectral response acceleration of 1.37 seconds and 0.869 seconds for 0.2 and 1-second, respectively, with a 5% damping ratio.

Finite element model

CSI sap2000 was used as a finite element (FE) software program to create a 3D nonlinear Finite Element (FE) model of the petrochemical plant structure, which included nonlinear hinges at both ends of the elements to simulate the behaviour of the structure in the nonlinear region. The hinges included axial load-bending P-M2-M3 hinges to model the coupled axial and bending behaviour in columns, as well as bending hinges (M3) to simulate the bending behaviour of the beams, as per the guidelines set out in the ASCE/SEI 41-13, (2014) standard. Also, the axial hinges were chosen to simulate the buckling behaviour of the bracing frames. The model is illustrated in Fig. 2.

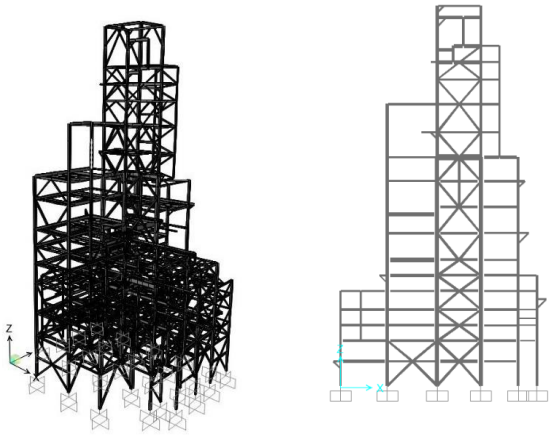

Figure 2. The finite element model.

Damage assessment

To make a risk-management decision, it is important to evaluate the probability of damage to the structure during earthquakes of varying intensity levels. A useful method for assessing the behaviour of the structure in both linear and nonlinear regions is the use of incremental dynamic analysis (Vamvatsikos and Allin Cornell, 2002). Incremental dynamic analysis (IDA) is a multi-level, multi-scale analysis technique that assesses the structural response of a building under various levels of ground motion intensity. It involves a series of nonlinear dynamic analyses, gradually increasing the intensity of the input ground motion, to achieve different performance levels and damage states. The fragility curves then can be extracted based on the results of the IDA analysis. In this study, spectral acceleration at the dominant-mode period of the structure, $S_a(T_s)$, was selected as a sensitive ground motion intensity measure (IM), and the maximum inter-story drift ratio (MIDR) as an engineering demand parameter (EDP) was chosen to reflect the extent of damage at each IM level.

Seismic fragility analysis is an effective method for evaluating the seismic performance of a structure based on the probability of failure as a function of IM in which failure is defined with respect to damage states (DS) (Muntasir Billah and Shahria Alam, 2014) .Under the assumption of a lognormal distribution between EDP and IM, the fragility curve can be represented by the

probability of reaching or exceeding the damage limit state (ds_i) for a given level of seismic excitation (IM). The following distribution represents the fragility function.

$$\mathrm{P}\left[\mathrm{DS} \geq \mathrm{ds}_i | \mathrm{IM} = \mathrm{x}\right] = \Phi\left(\frac{\ln(im/\theta i)}{\beta i}\right) \quad (1)$$

where $\mathrm{P}\left[\mathrm{DS} \geq \mathrm{ds}_i | \mathrm{IM} = \mathrm{x}\right]$ is the probability of damage at each damage state (ds_i), which is calculated using the cumulative normal distribution function denoted by Φ. The parameters θ and β represent the median and standard deviation of the natural logarithm of the structure's capacity at damage state i, respectively.

Seismic hazard definition and input ground motions

Hazard curves are used to characterize the ground motion activities at a specific location, providing information on earthquake frequency at various intensity measure (IM) levels. This data can be collected through past investigations or a probabilistic seismic hazard assessment. To assess the risk, fragility functions can be integrated with the hazard curve, allowing for the calculation of the annual failure rate of different degrees of damage. In this study, the hazard curve for the site of the case study is shown in Fig. 3 (Karagiannakis et al., 2022).

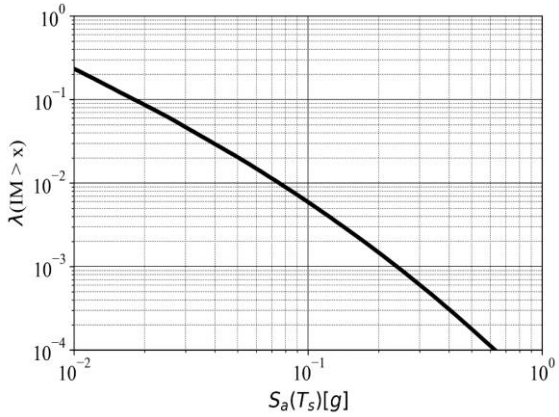

Figure 3. Seismic hazard curve of the case study region.

The seismic evaluation of the structure involved using a range of ground motion records, including 22 far-field and 28 near-field records, selected based on the Federal Emergency Management Agency report (FEMA P-695). These records were employed as input for the intensity measure (IM) in the structural analysis. These inputs were then used to develop fragility functions, allowing for the assessment of the risk associated with seismic activity in the case study region.

Annual failure rate and loss exceedance curve

The annual failure rate is an essential metric in risk assessment and can help in developing effective strategies for hazard mitigation and management and evaluating the safety of a structure. The probability of failure for each potential damage state can be calculated for different levels of input intensity measures (IMs) considering the hazard characteristics of the structure region. The annual failure rate is a measure of the average number of failures expected to occur in a year at a specific IM. As illustrated in Eq.(6), This can be determined by combining the hazard curve and fragility function in a discrete format.

$$\lambda(\mathrm{C} > \mathrm{c}) = \sum_{i=1}^{n} P(C > c | IM = \mathrm{x}_i) * \Delta\lambda_i \quad (6)$$

where λ(F) represents the annual failure rate, reaching a particular damage state, $P(C > c|IM = \mathrm{x}_i)$ the probability of the structure reaching a certain damage state given the input IM level x_i, by the difference between the hazard curve values at each discrete IM level, $\Delta\lambda_i$.

Results and discussion

Modal analysis

Table 2 presents the frequencies of the structures in both corroded (C) and uncorroded (UC) conditions, which have the highest mass participation ratio. The most influential modes for the

uncorroded model were identified as mode 4 in the X direction and mode 3 in the Y direction. In contrast, for the corroded model, mode 17 was identified as the dominant mode in the X direction, while mode 16 was found to be the most critical in the Y direction.

Mode shape	Corrosion effect	Frequency (Hz)	Mass ratio (%)
4	UC	0.93	18.5
17	C	0.77	20.7
3	UC	0.85	18.5
16	C	0.70	20.4

Table 2. Modal analysis results for the main structure.

Damage limit states

Table 3 outlines the different levels of damage states based on the HAZUS standard thresholds. The initial loading stage, DS_1, is considered a light damage state, where minor damage such as small cracks and buckling of slender braces may be observed. As the intensity level increases, the damage state progresses to DS_2, denoted as moderate damage, where major cracks and noticeable buckling and stretching of braces can be seen. At the extensive damage state, which is the next level, most steel brace and members reach their yield strength capacity, resulting in significant and permanent deformations, and some members may even exceed their ultimate capacity, leading to a few collapses. Finally, the complete damage state is characterized by most structural elements reaching their ultimate capacity, and connections may fail, resulting in partial collapse of the structure.

Damage state (DS)	Damage level	MIDR [%]
DS_1	Light	0.30
DS_2	Moderate	0.60
DS_3	Extensive	1.50
DS_4	Complete	4.00

Table 3. Hazus structural damage limit states.

Fragility curves

Figure 4 presents the fragility curves for both the corroded and uncorroded structures subjected to near and far-field ground motion records. The solid lines represent the uncorroded model (UC), while the dashed lines show the corroded structure (C). The plot also includes the median (50th), 16th, and 84th percentiles to demonstrate the variability of the results. It is evident that there is a noticeable difference in the fragility curves between the corroded and uncorroded structures, which increases with increasing intensity levels ($S_a(T_s)$). Based on the median values (as shown in Fig. 4a & b), it can be inferred that the largest difference in the probability of damage between the corroded and uncorroded models occurs in the highest damage state (DS_4) which represents the nonlinear response of the structure at the higher damage level. Furthermore, the fragility curves for the far-field records indicate a lower probability of damage at a given intensity level compared to the near-field records. For instance, in case of far-field records (Fig.4-a), when a structure is subjected to $S_a(T_s)$= 2g, the probability of corrosion case damage is approximately 0.5 at 'Complete' damage state (DS_4), while it is approximately 0.1 in case of near-field records.

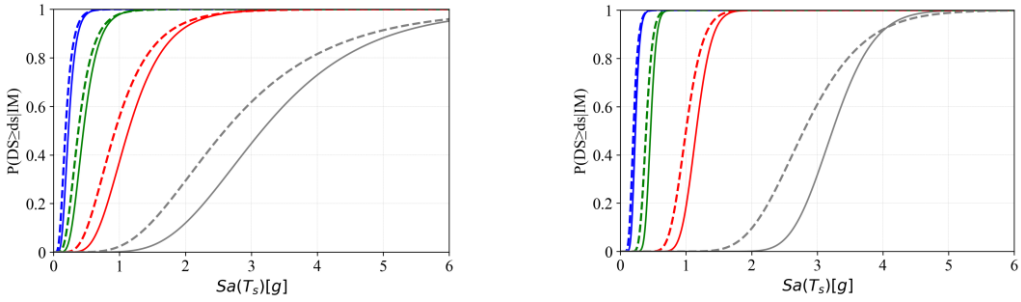

(a) (b)

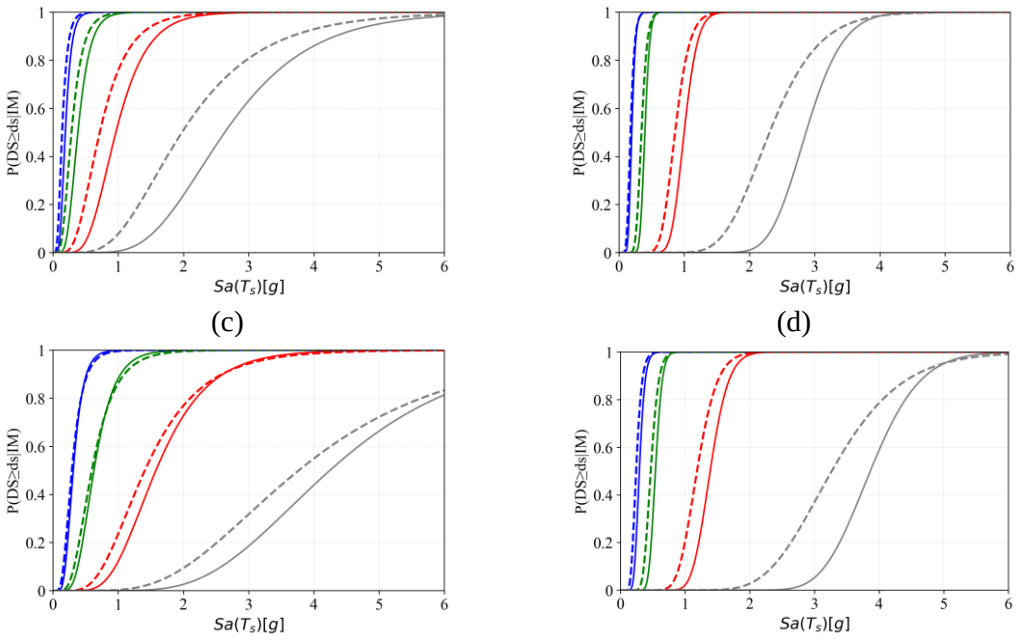

Figure 4. Fragility curves of (a) 50th, (c) 16th and (e) 84 percentile subjected to far-field records and (b) 50th, (d)16th and (f) 84 percentile for near-field motions.

Annual failure rate

The annual failure rate, λ(F), is plotted in Fig. 5 for each damage state level by combining the hazard characteristics into the fragility curve's results (see Fig.3 & 4 and Eq.6). The comparison between cases with and without corrosion reveals a small difference in the annual rate at the lowest damage level, but a significant difference at higher levels of damage.

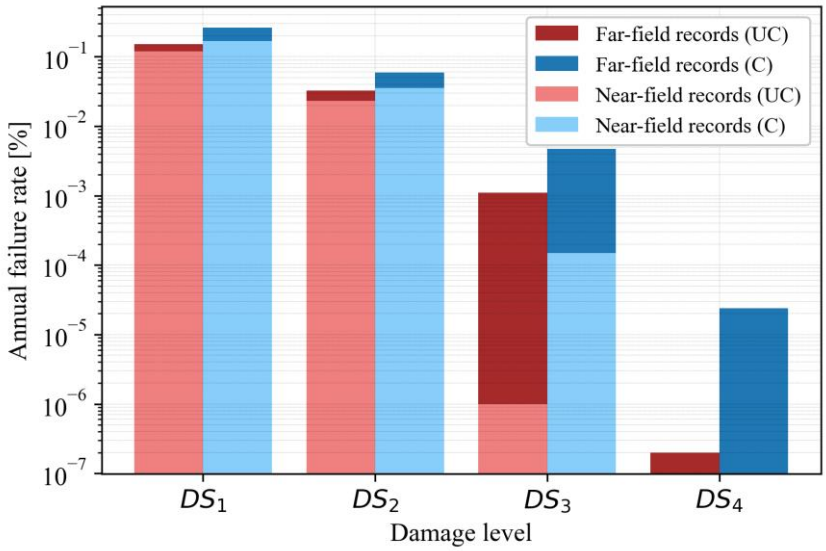

Figure 5. Annual failure rate ratio as a function of the damage states.

The results presented in Fig. 5 clearly demonstrate the impact of corrosion on the annual failure rate. For instance, in the case of far-field records, the annual failure rate for the corroded case was about 1.7 and 1.4 times higher than that of the uncorroded case in the first two damage states. At the extensive damage state (DS_3), the annual failure rate for the corroded case was approximately four times higher than that of the uncorroded case, while for complete damage (DS_4) level, the difference in higher. For near-field records, the difference in annual failure rate was around 150 times higher for damage state 3. It is worth noting that the hazard characteristics of the study region estimate the annual failure rate to be around 0 for damage state 4 on near-field records. Return periods can be estimated using the available annual failure rate data. For

instance, in the case of 'Moderate' damage state (DS_2), the estimated return period for the corroded structure is around 1689 years under far-field records, and around 2816 years under near-field records.

Conclusions and recommendations

This study examined the seismic risk assessment of a typical petrochemical building under harsh environmental conditions with high corrosivity level. The research used a real-world case study and developed fragility curves to determine the failure probability at various damage levels. The study also considered the hazard characteristics of the structure to determine the annual failure rate. The findings are summarized as follows: (1) The research found that corrosion has a significant impact on the probability of damage to the petrochemical building at all levels of severity. The fragility analyses conducted as part of the study revealed that the effect of corroded elements on the structural performance was more significant at higher levels of damage. In other words, the more severe the damage, the more critical it is to address the corrosion issue. (2) The fragility curves generated using far-field earthquake records show a lower probability of damage at a particular intensity level when compared to the fragility curves generated using near-field earthquake records. (3) The analysis of the annual failure rate at different levels of damage revealed that when the structure was subjected to far-field earthquake records, the rate of annual failure was higher compared to when it was subjected to near-field earthquake records. Moreover, the difference between the annual failure rate was significantly more pronounced at higher levels of damage. These results underscore the importance of considering the distance of the earthquake source when assessing the seismic risk of petrochemical buildings and implementing appropriate measures to mitigate the risk of damage.

The above findings can aid stakeholders and insurers in estimating damage and making informed decisions on retrofitting and proactive maintenance of aging petrochemical plants, enhancing their resilience against seismic events. Thus, implementing corrosion prevention and maintenance measures is critical to minimizing potential damage caused by corrosion in such structures.

References

Benarie, M., Lipfert, F.L., 1986. A general corrosion function in terms of atmospheric pollutant concentrations and rain pH. Atmospheric Environment (1967) 20, 1947–1958. https://doi.org/10.1016/0004-6981(86)90336-7

Koch, G., Varney, J., Thompson, N., Moghissi, O., Gould, M. and Payer, J., 2016. International measures of prevention, application, and economics of corrosion technologies study. NACE international, 216, pp.2-3..

Elchalakani, M., 2016. Rehabilitation of corroded steel CHS under combined bending and bearing using CFRP. J Constr Steel Res 125, 26–42. https://doi.org/10.1016/J.JCSR.2016.06.008

Evaluation of the FEMA P-695 Methodology for Quantification of Building Seismic Performance Factors | NIST [WWW Document], n.d. URL https://www.nist.gov/publications/evaluation-fema-p-695-methodology-quantification-building-seismic-performance-factors?pub_id=915492.

Helsel, J.L. and Lanterman, R., 2022, March. Expected service life and cost considerations for maintenance and new construction protective coating work. In AMPP Annual Conference+ Expo. OnePetro.

Feliu, S., Morcillo, M., Feliu, S., 1993a. The prediction of atmospheric corrosion from meteorological and pollution parameters—II. Long-term forecasts. Corros Sci 34, 415–422. https://doi.org/10.1016/0010-938X(93)90113-U

Feliu, S., Morcillo, M., Feliu, S., 1993b. The prediction of atmospheric corrosion from meteorological and pollution parameters—I. Annual corrosion. Corros Sci 34, 403–414. https://doi.org/10.1016/0010-938X(93)90112-T

ISO, I., 9223: 2012: Corrosion of Metals and Alloys—Corrosivity of Atmospheres—Classification. Determination and Estimation.

ISO, B., 2012. BS EN ISO 9224: 2012. Corrosion of metals and alloys–Corrosivity of atmospheres–Classification, determination and estimation.

Jagtap, P.R. and Pore, S.M., 2021. Strengthening of fully corroded steel I-beam with CFRP laminates. Materials Today: Proceedings, 43, pp.2170-2175. https://doi.org/10.1016/J.MATPR.2020.12.106

Kallias, A.N., Imam, B., Chryssanthopoulos, M.K., 2016. Performance profiles of metallic bridges subject to coating degradation and atmospheric corrosion. https://doi.org/10.1080/15732479.2016.1164726 13, 440–453. https://doi.org/10.1080/15732479.2016.1164726

Karagiannakis, G., Di Sarno, L., Necci, A., Krausmann, E., 2022. Seismic risk assessment of supporting structures and process piping for accident prevention in chemical facilities. International Journal of Disaster Risk Reduction 69, 102748. https://doi.org/10.1016/J.IJDRR.2021.102748

Kee Paik, J., Kyu Kim, S., Kon Lee, S., 1998. Probabilistic corrosion rate estimation model for longitudinal strength members of bulk carriers. Ocean Engineering 25, 837–860. https://doi.org/10.1016/S0029-8018(97)10009-9

Kere, K.J., Huang, Q., 2019. Life-Cycle Cost Comparison of Corrosion Management Strategies for Steel Bridges. Journal of Bridge Engineering 24, 04019007. https://doi.org/10.1061/(asce)be.1943-5592.0001361

Landolfo, R., Cascini, L., Portioli, F., 2010. Modeling of Metal Structure Corrosion Damage: A State of the Art Report. Sustainability 2010, Vol. 2, Pages 2163-2175 2, 2163–2175. https://doi.org/10.3390/SU2072163

Hwang, H., Liu, J.B. and Chiu, Y.H., 2001. Seismic fragility analysis of highway bridges. https://doi.org/10.1080/15732479.2014.912243

Qin, S., Cui, W., 2003. Effect of corrosion models on the time-dependent reliability of steel plated elements. Marine Structures 16, 15–34. https://doi.org/10.1016/S0951-8339(02)00028-X

Rizzo, F., Di Lorenzo, G., Formisano, A., Landolfo, R., 2019. Time-Dependent Corrosion Wastage Model for Wrought Iron Structures. Journal of Materials in Civil Engineering 31, 04019165. https://doi.org/10.1061/(ASCE)MT.1943-5533.0002710

Seismic Evaluation and Retrofit of Existing Buildings, 2014. . Seismic Evaluation and Retrofit of Existing Buildings. https://doi.org/10.1061/9780784412855

Soares, G., Garbatov, Y., 1999. Reliability of maintained, corrosion protected plates subjected to non-linear corrosion and compressive loads. Marine Structures 12, 425–445. https://doi.org/10.1016/S0951-8339(99)00028-3

Vamvatsikos, D., Allin Cornell, C., 2002. Incremental dynamic analysis. Earthq Eng Struct Dyn 31, 491–514. https://doi.org/10.1002/EQE.141

Wang, H., Wang, Y., Zhang, Z., Liu, X., Xu, S., 2021. Cyclic behavior and hysteresis model of beam-column joint under salt spray corrosion environment. J Constr Steel Res 183, 106737. https://doi.org/10.1016/J.JCSR.2021.106737

Wang, H., Xu, S., Li, A., Kang, K., 2018. Experimental and numerical investigation on seismic performance of corroded welded steel connections. Eng Struct 174, 10–25. https://doi.org/10.1016/J.ENGSTRUCT.2018.07.057

Xu, S., Wang, H., Li, A., Wang, Y., Su, L., 2016. Effects of corrosion on surface characterization and mechanical properties of butt-welded joints. J Constr Steel Res 126, 50–62. https://doi.org/10.1016/J.JCSR.2016.07.001

Xu, S., Zhang, Z., Qin, G., 2019. Study on the seismic performance of corroded H-shaped steel columns. Eng Struct 191, 39–61. https://doi.org/10.1016/J.ENGSTRUCT.2019.04.037

Yousefi, O., Narmashiri, K., Hedayat, A.A., Karbakhsh, A., 2021. Strengthening of corroded steel CHS columns under axial compressive loads using CFRP. J Constr Steel Res 178, 106496. https://doi.org/10.1016/J.JCSR.2020.106496